

# Resonant response of spar-type floating platform in coupled heave and pitch motion

E.Y. Choi<sup>1</sup>, J.R. Cho<sup>\*2</sup> and W.B. Jeong<sup>3</sup>

<sup>1</sup>KFX Airframe Analysis Team, Korea Aerospace Industries, Sacheon 52529, Republic of Korea

<sup>2</sup>Department of Naval Architecture and Ocean Engineering, Hongik University, Sejong 339-701, Republic of Korea

<sup>3</sup>School of Mechanical Engineering, Pusan National University, Busan 609-735, Republic of Korea

(Received April 14, 2017, Revised September 28, 2017, Accepted October 28, 2017)

**Abstract.** In this paper, the resonance response of spar-type floating platform in coupled heave and pitch motion is investigated using a CPU time-effective numerical method. A coupled nonlinear 2-DOF equation of motion is derived based on the potential wave theory and the rigid-body hydrodynamics. The transient responses are solved by the fourth-order Runge-Kutta (RK4) method and transformed to the frequency responses by the digital Fourier transform (DFT), and the first-order approximation of heave response is analytically derived. Through the numerical experiments, the theoretical derivation and the numerical formulation are verified from the comparison with the commercial software AQWA. And, the frequencies of resonance arising from the nonlinear coupling between heave and pitch motions are investigated and justified from the comparison with the analytically derived first-order approximation of heave response.

**Keywords:** spar-type floating platform; heave and pitch motions; coupled nonlinear equations; coupled resonance response; resonance frequencies; first-order approximation

## 1. Introduction

Floating platforms are widespread in the field of ocean engineering, such as floating offshore wind turbines (Wang *et al.* 2016). Among various types of floating platforms, spar-type is commonly preferred due to its excellent strength of vertical posture stability and the relatively easy installation at deep sea (Choi *et al.* 2015). But, since it suffers from the structural vibration stemming from wave load at the same time, because it is not fixed on ground but floating by buoyancy (Irani and Finn 2004, Jeon *et al.* 2013, Browning *et al.* 2014). Here, the structural vibration is mostly meant by the pitch and roll motions and the heave motion in the vertical direction.

Therefore, the securing of dynamically stable vertical posture by suppressing the structural vibration is essential for the successful application of spar-type floating platform in the ocean engineering field. It is because the vertical posture instability may cause the fatal structural failure that leads to the tremendous loss of financial, environmental and human resources. In order to prevent such an incident at sea, the designer has to investigate its structural dynamic responses, particularly the resonance response, to diverse wave conditions. In this connection, the extensive studies are carrying out to investigate the dynamic behavior of floating platform, which includes the cost- and time-consuming experimental studies using scale models (Utsunomiya *et al.* 2009, Olinger *et al.* 2012) and the

complex numerical simulations by utilizing the fluid-structure interaction scheme (Agamloh *et al.* 2008, Jeon *et al.* 2013).

Compared with other floating platforms, the water plane area of spar-type floating platforms is smaller than the submerged area. So, the small restoring stiffness in the vertical direction causes a large perpendicular motion at resonance when subject to external vibrations, which gives rise to a negative effect on self-aligning moment (Karimirad *et al.* 2011). The change in self-aligning moment in the horizontal direction contributes to the time delay in vertical motion and results in the phase change. The stability of floating platforms in such a coupled motion was assessed based on the Mathieu-type equation (Haslum and Faltinsen 1999), which is a topic that has been extensively studied. And, the resonance responses were investigated either by experimental model tests or by numerical simulations based on finite element method or steady-state bifurcation.

Rho *et al.* (2002, 2004), in their model tests of coupled motion in the heave and pitch directions of floating platforms using a wave tank, found that the coupling in resonance occurs with unstable pitch motion when the natural frequency of pitch becomes twofold that of wave frequency, and the frequency of vibrations approaches the natural frequency of heave motion. Hong *et al.* (2005) conducted a test involving regular wave excitation at different frequencies by manufacturing a floating substructure test model, and they verified that, when the excitation frequency was close to the heave natural frequency or a value twice that of the pitch natural frequency, the combination resonance occurs due to an unstable pitch motion. Zhao *et al.* (2010) obtained the steady-state heave and pitch responses by solving the

---

\*Corresponding author, Professor  
E-mail: jrcho@hongik.ac.kr

bifurcation equation, and they found a tripling of heave and pitch modes when the frequency of vibrations gets close to the sum of the heave and pitch natural frequencies. Matos *et al.* (2011) computed the second-order resonant heave, roll and pitch motions by means of a commercial BEM code and compared with those measured in small-scale tests performed in a wave basin.

The purpose of the current study is to numerically investigate the coupled response of spar-type floating platform in heave and pitch motions using a CPU time-effective numerical method. A spar-type floating platform in 2-D surface wave is assumed to be a rigid body having 2-DOFs, and its coupled nonlinear equations of motion are derived based on the wave potential theory and the rigid-body hydrodynamics. The hydrodynamic interaction between the wave flow and the rigid floating platform is reflected by means of the added mass and added inertia of moment. The transient heave and pitch responses are solved by the fourth-order Runge-Kutta (KR4) method and transformed to the frequency responses by the digital Fourier transform (DFT). The theoretical derivation and the numerical formulation are verified by comparing the frequency responses with Ansys AQWA (Ansys 2012), and the resonance frequencies are investigated and justified from the comparison with the analytically derived first-order approximation of heave response.

### 2. Spar-type floating platform in 2-D surface wave

Referring to Fig. 1, let us consider 2-D incompressible, irrotational and inviscid surface wave of the wave length  $\lambda$ , the wave amplitude  $\eta_a$  and the mean water depth  $h$ . The unsteady flow velocity  $\mathbf{v} = \{u, w\}$  of water particles is governed by the Bernoulli equation (Currie 1974) expressed by

$$\frac{1}{2}(u^2 + w^2) + \frac{p}{\rho} + gz + \frac{\partial\phi}{\partial t} = 0 \quad (1)$$

with the velocity potential  $\phi(x, z)$ . Here, the velocity potential is due to the rigid body motion of platform and the undisturbed incoming wave, by considering only the hydrostatic restoring effect. In other words, the hydrodynamic effects, i.e., the second-order wave excitations from wave-body interaction including diffraction and radiation effects, are neglected. This simplification would influence the prediction accuracy of response amplitude of platform (Kriebel 1998, Dalzell 1999, Wang and Wu 2007). The flow velocity satisfies the non-penetration condition given by

$$w = \frac{\partial\phi}{\partial z} = 0 \text{ at } z = -h \quad (2)$$

at the bottom surface, and the kinematic boundary condition given by

$$w = \frac{\partial\eta}{\partial t} + u \frac{\partial\eta}{\partial x} \text{ at } z = \eta(x; t) \quad (3)$$

and the dynamic boundary condition:

$$\frac{1}{2}(u^2 + w^2) + g\eta + \frac{\partial\phi}{\partial t} = 0 \text{ at } z = \eta(x; t) \quad (4)$$

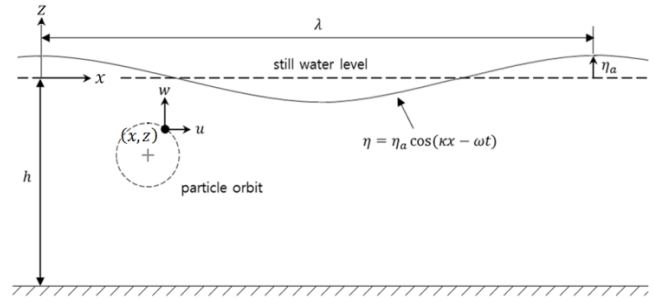


Fig. 1 2-D progressive surface wave

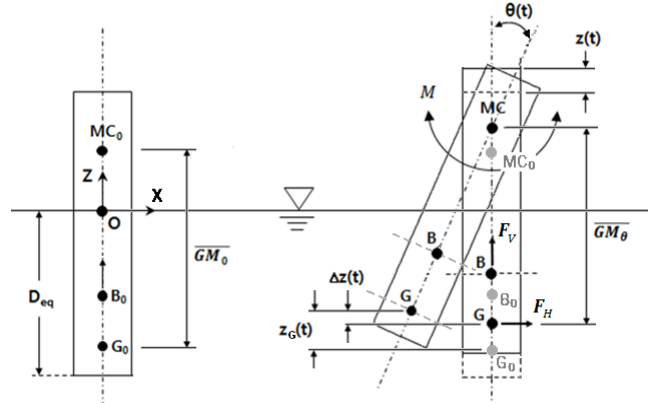


Fig. 2 A spar-type floating platform in heave and pitch motions

with  $\rho$  and  $g$  being the water density and the gravitational acceleration. The wave height  $\eta = \eta(x; t)$  in 2-D surface wave is defined by  $\eta(x; t) = \eta_a \cos(\kappa x - \omega t)$  with  $\kappa$  being the wave number. In case of the small amplitude sloshing flow, the two boundary conditions in Eqs. (3) and (4) at the free surface can be simplified as

$$w = \frac{\partial\eta}{\partial t} \text{ at } z = 0 \quad (5)$$

$$g\eta + \frac{\partial\phi}{\partial t} = 0 \text{ at } z = 0 \quad (6)$$

by neglecting the high-order terms.

Fig. 2 represents a 2-D cylindrical floating platform in heave and pitch motions, where O is the origin of Cartesian co-ordinates and  $D_{eq}$  is the draft (i.e., the length of wet part). The center of buoyancy, the center of gravity and the metacenter at the static equilibrium are denoted by  $B_0$ ,  $G_0$  and  $MC_0$ , while three points at the current state are indicated by  $B$ ,  $G$  and  $MC$ . The platform is assumed to be a rigid undamped body with two degrees-of-freedom. Letting  $\mathbf{F} = \{F_H, F_V\}$  and  $M$  be the hydrodynamic force and moment resultants, the heave motion  $z(t)$  and pitch motion  $\theta(t)$  around the metacenter  $MC$  are governed by

$$m\ddot{z}(t) + k \cdot z(t) = F_V \quad (7)$$

$$I\ddot{\theta}(t) + k_\theta \cdot \theta(t) = M \quad (8)$$

with  $m$  and  $I$  being the total mass and the moment of inertia. Here, the moment of inertia  $I$  of floating platform is defined with respect to the metacenter so that it varies with the motion of floating platform. Meanwhile, the hydrostatic

stiffnesses  $k$  and  $k_\theta$  in the heave and pitch motions are defined by

$$k = \rho g A_w \quad (9)$$

$$k_\theta = \rho g \nabla \cdot \overline{GM}_\theta \quad (10)$$

with the waterplane area  $A_w$  and the metacentric height  $\overline{GM}_\theta$ . Here, the displacement volume  $\nabla$  (i.e., the volume of submerged part) is calculated by

$$\nabla = A_w \times (D_{eq} - z) \quad (11)$$

Note that  $k_\theta$  is not constant but variable because both  $\nabla$  and  $\overline{GM}_\theta$  are varying with the motion of floating platform.

From the geometric configuration of the floating platform, the heave displacement  $z(t)$  at the metacenter  $MC$  and the heave displacement  $z_G(t)$  at the center of gravity are in the following relationship given by

$$z(t) = z_G(t) - \Delta z(t) \quad (12)$$

$$= z_G(t) - 2 \cdot \overline{GM}_\theta \cdot \sin^2\left(\frac{\theta(t)}{2}\right)$$

The volume change of submerged part according to the platform motion results in the position change of the center of buoyancy, which in turn changes the metacenter. Hence, the metacentric height  $\overline{GM}_\theta$  at the pitch angle  $\theta$  is determined from the following relation given by

$$\begin{aligned} \overline{GM}_\theta &= \overline{GMC}_0 + \overline{MC}_0 \overline{MC} \\ &= \overline{GM}_0 + \frac{1}{2} \cdot \frac{I_w}{\nabla} \cdot \tan^2 \theta \end{aligned} \quad (13)$$

with  $I_w$  being the area moment of inertia of the wet part of floating platform.

Substituting Eq. (13) into Eq. (12), together with the approximation of  $\sin^2 \theta = \tan^2 \theta \approx \theta^2$  for small rotation, ends up with

$$\begin{aligned} z(t) &= z_G(t) - \left( \overline{GM}_0 + \frac{1}{2} \cdot \frac{I_w}{\nabla} \cdot \theta^2 \right) \cdot \frac{\theta^2}{2} \\ &= z_G(t) - \overline{GM}_0 \cdot \frac{\theta^2}{2} \end{aligned} \quad (14)$$

$$\ddot{z}(t) = \ddot{z}_G(t) - \overline{GM}_0 \cdot (\dot{\theta}^2 + \theta \ddot{\theta}) \approx \ddot{z}_G(t) \quad (15)$$

By substituting the approximate equations (Eqs. (14) and (15)) into the equation of translation motion (1), one can derive the following approximate equation of heave motion given by

$$m \ddot{z}_G(t) + k \left( z_G(t) - \overline{GM}_0 \cdot \frac{\theta^2}{2} \right) = F_V \quad (16)$$

at the center of gravity. Furthermore, by substituting Eq. (10) into Eq. (8), using the relations in Eqs. (11)-(13), one can derive the approximate equation of pitch motion, which is given by

$$\begin{aligned} I \ddot{\theta}(t) + k \cdot D_{eq} \cdot \overline{GM}_0 \cdot \theta(t) + \frac{1}{2} \left( k \cdot \overline{GM}_0^2 + \rho g I_w \right) \cdot \\ \theta^3 - k \cdot \overline{GM}_0 \cdot z_G(t) \cdot \theta(t) = M \end{aligned} \quad (17)$$

Then, finally Eqs. (16) and (17) can be integrated into the following matrix form of coupled equations for  $z_G(t)$

and  $\theta(t)$

$$\begin{bmatrix} \tilde{m} & 0 \\ 0 & \tilde{I} \end{bmatrix} \begin{Bmatrix} \ddot{z}_G \\ \ddot{\theta} \end{Bmatrix} + \begin{bmatrix} k & -\frac{1}{2} \cdot \overline{GM}_0 \cdot \theta \\ -k \cdot \overline{GM}_0 \cdot \theta & \tilde{k} \end{bmatrix} \begin{Bmatrix} z_G \\ \theta \end{Bmatrix} = \begin{Bmatrix} F_V \\ M \end{Bmatrix} \quad (18)$$

with  $\tilde{m} = m + m_a$ ,  $\tilde{I} = I + I_a$  and  $\tilde{k} = k \cdot D_{eq} \cdot \overline{GM}_0 + \frac{1}{2} \left( k \cdot \overline{GM}_0^2 + \rho g I_w \right) \cdot \theta^2$ . Here,  $m_a$  and  $I_a$  indicate the added mass in heave motion and the added moment of inertia in pitch motion. The floating platform and wave flow engage in mutual interactions through the shared common interface, and this hydrodynamic effect is reflected in the form of added mass. It is known that the added mass is dependent of structural motion as well as the wave frequency (Cho *et al.* 2001, Kim *et al.* 2002). The transient response of Eq. (18) is solved using the fourth-order Runge-Kutta (RK4) method which is numerically implemented by MATLAB.

### 3. Hydrodynamic force and moment

Assuming 2-D surface wave be small-amplitude, one can drive the wave velocity potential given by

$$\phi = \eta_a \cdot \frac{g}{\omega} \cdot \frac{\cosh[\kappa(h+z)]}{\cosh(\kappa h)} \sin(\kappa x - \omega t) \quad (19)$$

from the governing Eqs. (1)-(4) (Dean and Dalrymple 1984). Then, from the definition of wave velocity potential, one can drive the directional particle velocities given by

$$u = \frac{\partial \phi}{\partial x} = \eta_a \cdot \frac{\kappa g}{\omega} \cdot \frac{\cos[\kappa(h+z)]}{\cosh(\kappa h)} \cdot \cos(\kappa x - \omega t) \quad (20)$$

$$w = \frac{\partial \phi}{\partial z} = \eta_a \cdot \frac{\kappa g}{\omega} \cdot \frac{\sinh[\kappa(h+z)]}{\cosh(\kappa h)} \cdot \sin(\kappa x - \omega t) \quad (21)$$

Substituting the velocity potential  $\phi$  into the modified kinematic boundary condition:  $\frac{\partial^2 \phi}{\partial t^2} + g \frac{\partial \phi}{\partial z} = 0$  at the mean surface ( $z = 0$ ), one can get the dispersion relationship which is expressed in terms of the frequency  $\omega$  and the wave number  $\kappa$

$$\omega^2 = \kappa g \cdot \tanh(\kappa h) \quad (22)$$

In case of deep water ( $h \rightarrow \infty$ ), the term  $\tanh(\kappa h)$  approaches unity and the hyperbolic function terms in Eqs. (19)-(21) become  $\exp(\kappa z)$ , which leads to the following directional water particle velocities given by

$$u = \eta_a \omega \cdot e^{\kappa z} \cdot \cos(\kappa x - \omega t) \quad (23)$$

$$w = \eta_a \omega \cdot e^{\kappa z} \cdot \sin(\kappa x - \omega t) \quad (24)$$

According to the Bernoulli equation, one can drive the wave pressure field  $p(x, z, t)$  given by

$$p(x, z, t) = -\frac{1}{2} \rho \eta_a^2 \omega^2 \cdot e^{2\kappa z} + \rho g \eta \cdot e^{\kappa z} \cdot \cos(\kappa x - \omega t) \quad (25)$$

Where, the hydrostatic pressure term  $\rho g z$  was excluded because it is considered as the initial condition for the hydrodynamic analysis.

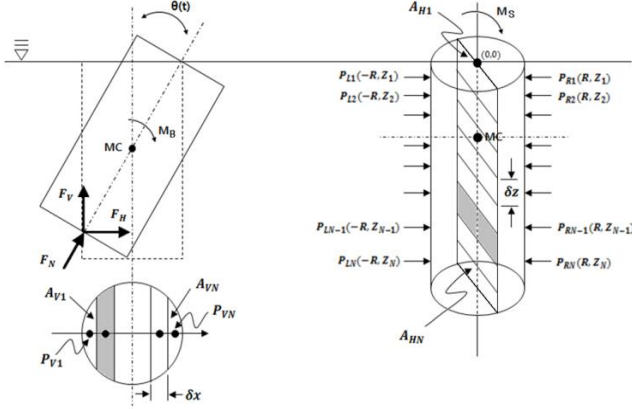


Fig. 3 Free body diagram of the floating platform subject to the hydrodynamic pressure

Next, we calculate the force and moment resultants that are produced by the hydrodynamic pressure  $p(x, z; t)$  acting on the surface of floating platform. Fig. 3 shows the free body diagram of floating platform, where the radius and the cross-section are denoted by  $R$  and  $A_V$ , respectively. The surface of floating platform is composed of the bottom surface  $B$  and the cylindrical surface  $S$ , and the normal force resultant  $F_N$  is acting on  $B$  while the hydrodynamic pressure acting on  $S$  is projected on the left and right sides of the vertical cross-section normal to the wave direction. The heave motion is caused by the vertical force resultant force  $F_V$ , while the pitch motion is induced by  $M_B$  and  $M_S$ . To calculate the force and moment resultants, the bottom surface and the cylindrical surface are equally divided into  $N$  sub-sections. Each cross-section is assumed to be subject to a force amounting to the central pressure multiplied by its area. For the division  $i = 1 \sim N$ , the sub-sectional areas  $A_{Vi}$  and  $A_{Hi}$  on the bottom surface and the projected vertical cross-section are calculated by

$$A_{Vi} = 2 \cdot \sqrt{R^2 - x^2} \cdot dx \quad (26)$$

$$A_{Hi} = 2 \cdot R \cdot \delta z \quad (27)$$

Meanwhile, the co-ordinates  $(x_i, z_i)$  of the sampling points within each sub-section are determined by the geometry transformation between the static equilibrium state and the current moving state. Letting  $(X_i, Z_i)$  be the sampling points at the static equilibrium and  $(0, b)$  be the co-ordinates of metacenter  $MC$  at the current moving state, the following geometric transformation

$$x_i = X_i \cdot \cos \theta(t) - (Z_i - b) \cdot \sin \theta(t) \quad (28)$$

$$z_i = X_i \cdot \sin \theta(t) + (Z_i - b) \cdot \cos \theta(t) + z(t) \quad (29)$$

According to the translational heave motion  $z(t)$  and the rotational pitch motion  $\theta(t)$ .

The hydrodynamic pressure at a specific position  $(x', z')$  on the surface of floating platform under heave and pitch motions is calculated by

$$p(x', z'; t) = -\frac{1}{2} \rho \eta^2 \omega^2 \cdot e^{2\kappa z'} + \rho g \eta \cdot e^{\kappa z'} \cdot \cos(\kappa x' - \omega t) \quad (30)$$

Referring to Fig. 3, the normal force  $F_{Ni}$  acting on the  $i$ -th cross-section of platform bottom surface  $B$  is calculated by

$$F_{Ni} = p(P_{Vi}; t) \cdot A_{Vi} \quad (31)$$

Then, the vertical force component  $F_{Vi}$  and the horizontal force component  $F_{Hi}$  are expressed by

$$F_{Vi} = F_{Ni} \cdot \cos \theta(t) \quad (32)$$

$$F_{Hi} = F_{Ni} \cdot \sin \theta(t) \quad (33)$$

Thus, the moment  $M_B$  due to the hydrodynamic pressure acting on the bottom surface  $B$  becomes the sum of all the contributions of  $N$  cross-sections as follows

$$M_B = \sum_{i=1}^N [F_{Vi} \cdot (P_{Vxi} - MC_x) + F_{Hi} \cdot (P_{Vzi} - MC_z)] \quad (34)$$

with  $(P_{Vxi}, P_{Vzi})$  and  $(MC_x, MC_z)$  being the positions of  $P_{Vi}$  and the metacenter  $MC$ .

Meanwhile, on the  $i$ -th cross section  $A_{Hi}$  of the cylindrical surface  $S$  of floating platform, the left and right force components  $F_{Li}$  and  $F_{Ri}$  are calculated by

$$F_{Li} = p(P_{Li}; t) \cdot A_{Hi} \cdot \cos \theta(t) \quad (35)$$

$$F_{Ri} = p(P_{Ri}; t) \cdot A_{Hi} \cdot \cos \theta(t) \quad (36)$$

Then, the moment  $M_S$  arising from the difference in the hydrodynamic pressures on the left and right sides can be calculated according to

$$M_S = \sum_{i=1}^N F_{Ri} \cdot (P_{Rzi} - MC_z) - \sum_{i=1}^N F_{Li} \cdot (P_{Lzi} - MC_z) \quad (37)$$

with  $P_{Rzi}, P_{Lzi}, MC_z$  being the  $z$  components of  $P_{Ri}, P_{Li}$  and  $MC$  respectively.

Finally the vibratory force  $F_V$  causing the heave motion and the total moment  $M$  acting on the floating platform become

$$F_V = \sum_{i=1}^N F_{Vi}, \quad M = M_B + M_S \quad (38)$$

#### 4. Numerical results

To verify the transient response solved by the fourth-order RK method with the help of MATLAB, the hydrostatic and hydrodynamic analysis was also performed with the same model using the commercial software AQWA. In case of AQWA, the motion platform motion is expressed in terms of three rigid body translations and three rigid body rotations. The wave flow is assumed to be ideal flow, and its velocity potential is contributed to the platform motion, the undisturbed incoming wave and the diffraction of incoming wave (Jeon *et al.* 2013). Fig. 4 represents a computation grid and the major simulation parameters that are set for the transient analysis using AQWA. The total number of surface elements is 3,118 and the wave amplitude and frequency are set the same as the present method.

The interaction between the wave potential flow and the platform rigid body motion is solved by the panel method

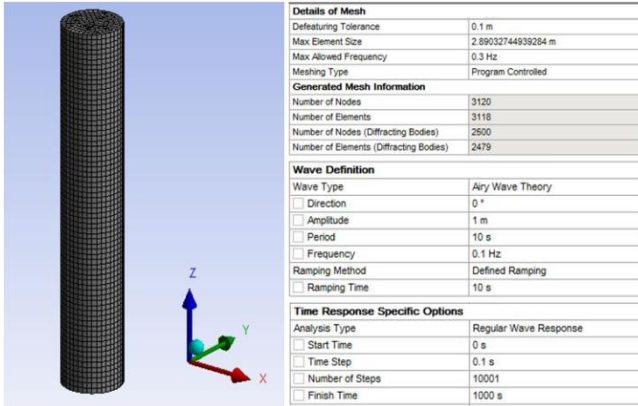


Fig. 4 Computation grid and the major parameter setting for Ansys AQWA

Table 1 Input parameters for the hydrostatic analysis using Ansys AQWA

Items	Values
Water density, $\rho$ [ $kg/m^3$ ]	1025
Wave height, $\eta$ [ $m$ ]	1.0
Mass of platform, $m$ [ $kg$ ]	31,974,000
Radii of gyration, $K_{xx}$ , $K_{yy}$ , $K_{zz}$ , [ $m$ ]	0.01, 0.01, 10.6
Cylinder radius, $R$ [ $m$ ]	10
Point mass location, $(x, y, z)$ [ $m$ ]	(0, 0, -60)

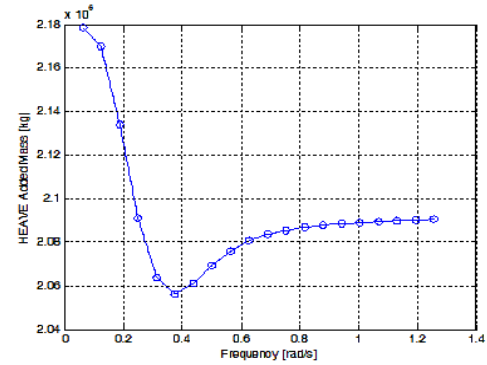
(Sahin 1997). For the rigid body dynamic analysis, only the surface of floating platform is discretized with 2-D finite elements as shown in Fig. 4. On the other hand, the rigid body motion in the present method is represented with only 2-DOFs and the hydrodynamic effect of wave on the floating platform is reflected by simply calculating the force and moment resultants that are resulted from the wave potential flow. Thus, the present method is highly CPU time-effective such that it takes only five minutes to solve the coupled Eq. (18), when compared with the transient analysis using AQWA requiring almost one hour.

#### 4.1 Hydrostatic results

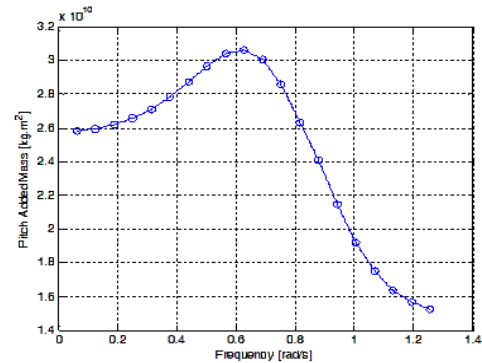
The state of static equilibrium was first calculated, and the results were used as initial values for the hydrodynamic analysis. The parameters taken for the analysis are given in Table 1, where the radii of gyration are given to construct a 2-D analysis model from the original 6-DOF one. The value 10.6 [ $m$ ] of  $K_{zz}$  indicates the distance from the mass center to the center of rotation (i.e., the metacenter). Table 2 compares the hydrostatic analysis results between AQWA and MATLAB for the same floating platform model. First of all, AQWA shows a smaller cut water plane area than MATLAB, which is caused in the course of constructing the lattices for the panel method in AQWA. In Table 2, the comparison shows the overall difference in the displacement volume and in the static rigidities in both the heave and pitch directions. To compensate for this difference, the parameters set for the numerical analysis model using MATLAB were adjusted to coincide with those set for AQWA.

Table 2 Comparison of the hydrostatic results between AQWA and MATLAB

Parameters		AQWA	MATLAB
Center of gravity, [ $m$ ]		(0,0,-60)	(0,0,-60)
Center of buoyancy, [ $m$ ]		(0,0,-49.647)	(0,0,-49.647)
Hydrostatic stiffness	Heave, [ $N/m$ ]	3,144,902	3,155,700
	Pitch, [ $N \cdot m/rad$ ]	$3.31 \times 10^9$	$3.32 \times 10^9$
Displacement volume, [ $m^3$ ]		31,066.045	31,194
Cut water plane area, [ $m^2$ ]		312.569	314.159
Metacentric height, [ $m$ ]		10.6037	10.6048



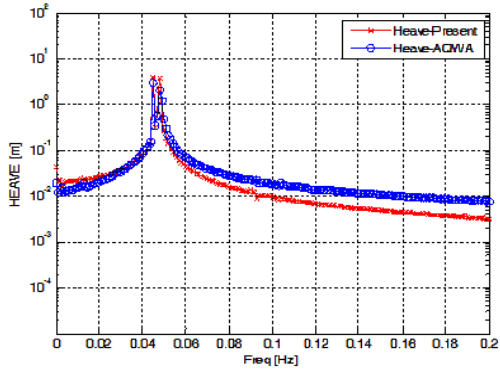
(a)



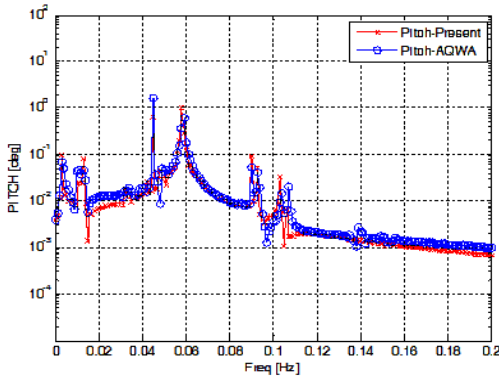
(b)

Fig. 5 Variation of added masses to the angular frequency: (a) in heave motion, (b) in pitch motion

The floating platform and wave flow engage in mutual interactions through the shared common interface, and this hydrodynamic effect is reflected in the form of added mass. It is known that the added mass is dependent of the frequency as well as the location and direction (Cho *et al.* 2001). Figs. 5(a) and 5(b) represent the frequency-dependent added masses in heave and pitch motions that were obtained by AQWA. By virtue of the fact that this study focuses on the resonance characteristics of the floating platform, the values of added mass at the heave and pitch natural frequencies are taken for the numerical experiments. The heave and pitch natural frequencies  $\omega_h$  and  $\omega_p$  of the above-mentioned AQWA model are 0.048[Hz] and 0.058[Hz] so that we have  $m_a = 2.07 \times 10^6$  kg and  $I_a = 2.78 \times 10^{10}$  kg  $\cdot$  m<sup>2</sup> from Fig. 5. One could derive the expressions of added mass based on the section theory for the structure of simple geometry.

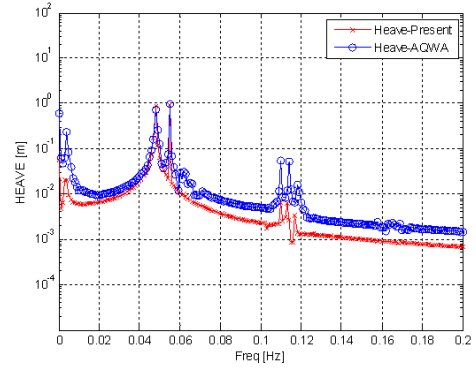


(a)

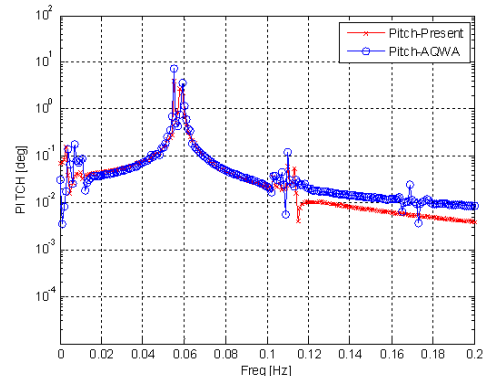


(b)

Fig. 6 Frequency responses when the wave frequency ( $\omega=0.045$  [Hz]) is slightly lower than the heave resonance frequency ( $\omega_h=0.048$  [Hz]): (a) heave, (b) pitch

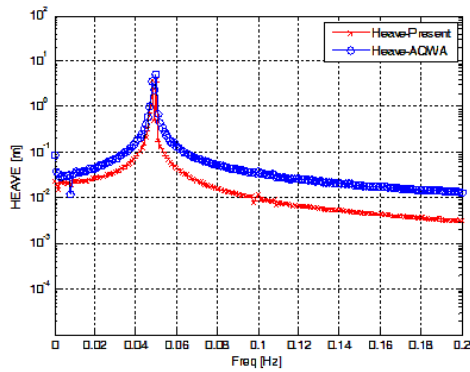


(a)

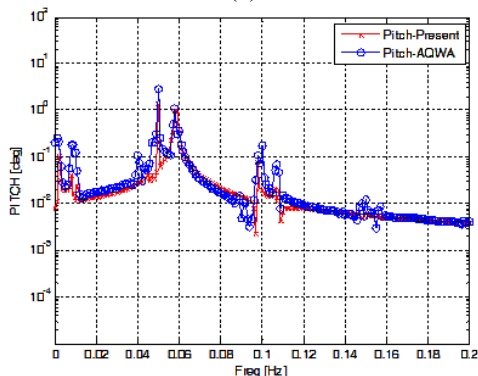


(b)

Fig. 8 Frequency responses when the wave frequency ( $\omega=0.055$  [Hz]) is slightly lower than the pitch resonance frequency ( $\omega_p=0.058$  [Hz]): (a) heave, (b) pitch

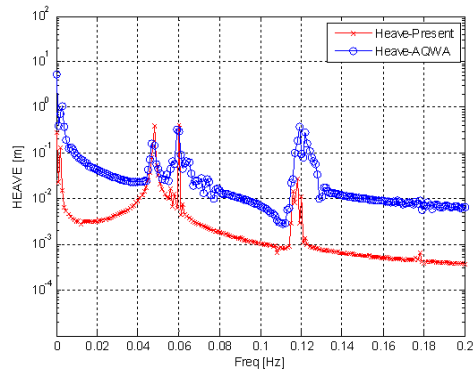


(a)

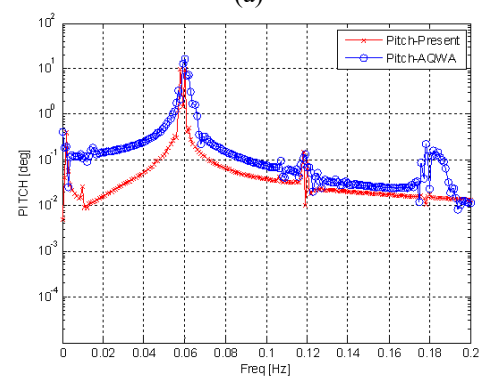


(b)

Fig. 7 Frequency responses when the wave frequency ( $\omega=0.05$  [Hz]) is slightly higher than the heave resonance frequency ( $\omega_h=0.048$  [Hz]): (a) heave, (b) pitch



(a)



(b)

Fig. 9 Frequency responses when the wave frequency ( $\omega=0.006$  [Hz]) is slightly higher than the pitch resonance frequency ( $\omega_p=0.058$  [Hz]): (a) heave, (b) pitch

Table 3 The frequencies showing the peaks in heave and pitch frequency responses to the excitation frequency using MATLAB

Exciting frequency $\omega$ [Hz]	Heave natural frequency $\omega_h$ [Hz]	Pitch natural frequency $\omega_p$ [Hz]	Double exciting Frequency $2\omega$ [Hz]	Other peak frequencies [Hz]
0.03			0.06	0.018, 0.028, 0.088
0.04			0.08	0.018, 0.08, 0.098
0.05			0.1	0.008, 0.098, 0.108
0.06			0.12	0.002, 0.118, 0.178
0.07	0.048	0.058	0.14	0.012, 0.116, 0.128
0.08			0.16	0.022, 0.116, 0.138
0.09			0.18	0.032, 0.116, 0.148
0.1			0.2	0.042, 0.116, 0.158

#### 4.2 Frequency response

The static equilibrium state in the hydrostatic analysis was used as the initial condition. The transient responses in the heave and pitch directions to a single regular wave were calculated using AQWA and a self-developed code in MATLAB and transformed into the frequency domain. The coupled resonance characteristics stemming from the coupling between heave and pitch motions were analyzed and compared. To investigate the resonance characteristics in relation to the frequency changes, particularly near the natural frequencies of heave and pitch motions, the analysis was performed while varying the wave frequency from 0.045[Hz] to 0.06[Hz] at 0.005[Hz] intervals. Figs. 6 to 9 show the frequency responses to when the wave frequency ( $\omega$ ) approaches the natural frequencies of heave ( $\omega_h = 0.048$ [Hz]) and pitch ( $\omega_p = 0.058$ [Hz]), respectively. Where, the horizontal axis indicates the frequency range of observation and the frequency responses obtained by the present method are observed to be slightly shifted as a whole. It is because the added masses taken for the present method are based on the fundamental heave and pitch natural frequencies.

Meanwhile, from Figs. 6-9, it is found that the present method gives the amplitudes that are smaller than those by AQWA. This difference was caused by the difference in modeling the wave excitation forces between the present method and AQWA. The present method considers only the contribution from the incident wave (i.e., the hydrostatic effect), as addressed in Section 2. On the other hand, the wave excitations in AQWA are computed by considering the wave diffraction and radiation (i.e., the hydrodynamic effects) as well as the undisturbed incoming wave (Ansys 2012). However, it is noted that any nonlinear hydrodynamic effect was not considered in AWQA.

By comparing the responses labeled by  $\ominus$  using AQWA with those labeled by  $\oplus$  using the self-developed code in MATLAB, one can clearly see the peaks at the heave and pitch natural frequencies and at the

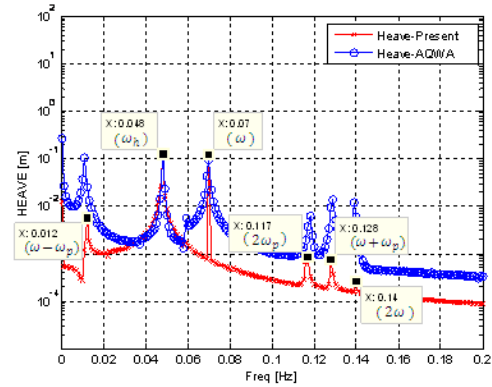


Fig. 10 The coupling in resonance in the heave frequency response (wave excitation frequency  $\omega=0.07$  [Hz])

excitation frequency. One can also observe the coupling in resonance at the other frequencies due to the coupling between heave and pitch motions. In order to clearly examine where the coupling in resonance occurs, the heave and pitch frequency responses were carried out by changing the excitation wave frequency from 0.03 Hz to 0.1 Hz with the increment of 0.01 Hz. Table 3 contains the frequencies where the peaks occur in heave or/and pitch motions with respect to the excitation frequency. Both heave and pitch frequency responses commonly show the peaks at the excitation frequency  $\omega$ , at the double excitation frequency  $2\omega$ , and at their own natural frequencies  $\omega_h$  and  $\omega_p$ , respectively. In addition, it was observed that the heave frequency responses show the peaks at the other frequencies.

Fig. 10 represents the heave frequency response at the excitation wave frequency  $\omega$  of 0.07 Hz, where  $X$  and  $Y$  stands for the resonance frequencies and the amplitudes. The peaks are observed at  $\omega (= 0.07$ [Hz]) and  $2\omega (= 0.14$ [Hz]) of the excitation frequency, at the heave natural frequency  $\omega_h (= 0.048$ [Hz]), at the double pitch natural frequency  $2\omega_p (= 0.117$ [Hz]), and at the frequencies  $\omega \pm \omega_p (= 0.012, 0.128$ [Hz]). Here, the peaks at the frequencies  $\omega \pm \omega_p$  are due to the coupling between heave and pitch motions. Hence, it is clearly found that the coupling in resonance occurs at the frequencies that are the sum and difference of the excitation frequency  $\omega$  and the natural frequency of pitch  $\omega_p$ . It is worth to note that the quadratic interactions (Pinkster 1980) of platform motions include these resonances from both hydrostatic restoring effect and hydrodynamic effects.

#### 5. Conclusions

In this study, the resonance response of spar-type floating platform in coupled heave and pitch motion was investigated using a CPU time-effective numerical method. A coupled nonlinear equations of motion for the spar-type floating platform in heave and pitch motions has been theoretically derived. The spar-type floating platform was simplified as a rigid body with two degrees of freedom, and the wave-platform interaction was taken into consideration

by means of the frequency-dependent added mass. And, the transient responses of the coupled nonlinear dynamic equations were solved by the fourth-order Runge-Kutta method, with the help of MATLAB, and those were transformed to frequency responses by DFT. The present numerical method was verified through the comparison with a commercial software AQWA, and the resonance frequencies arising from the coupling between heave and pitch motions were investigated. The main observations drawn from the numerical experiments are as follows:

1. The theoretical derivation of numerical formulation of coupled nonlinear equations, which were implemented by the RK4 method and DFT, lead to the frequencies that are in a good agreement with the results obtained using the commercial software AQWA.
2. The heave and pitch response commonly show the peaks at the excitation and double excitation frequencies as well as their own natural frequencies, regardless of the wave excitation frequency. In addition, the heave response show an additional peak at the double pitch natural frequency when the excitation frequency is higher than the pitch natural frequency.
3. Furthermore, the coupling in resonance arising from the coupling between heave and pitch motions occurs in the heave response at the specific frequencies; at the sum and difference  $\omega \pm \omega_p$  of the excitation frequency  $\omega$  and the pitch natural frequency  $\omega_p$  in the heave frequency response.
4. The resonance frequencies that were found from the present numerical method are consistent with those of the first-order approximation of heave response.

However, the current study was limited to regular wave so that the extension to irregular wave is needed to demonstrate the model capability. Furthermore, the validation of the theoretical work with experiment would be worthwhile, and which represents a topic that deserves future study.

## Acknowledgments

This work was supported by the Human Resources Development of the Korea Institute of Energy Technology Evaluation and Planning (KETEP) grant funded by the Korea Ministry of Knowledge Economy (No. 20113020020010). This work was supported by 2017 Hongik University Research Fund.

## References

- Agamloh, E.B., Wallace, A.K. and von Jouanne, A. (2008), "Application of fluid-structure interaction simulation of an ocean wave energy extraction device", *Renew. Energy*, **33**, 748-757.
- Ansys AQWA (2012), Available from: (<http://www.ansys.com/products/aqwa/>).
- Browning, J.R., Jonkman, J., Robertson, A. and Goupee, A.J. (2014), "Calibration and validation of a spar-type floating offshore wind turbine model using the FAST-dynamic simulation tool", *J. Phys. Conf. Ser.*, **555**, 012015.
- Cho, J.R., Song, J.M. and Lee, J.K. (2001), "Finite element techniques for the free-vibration and seismic analysis of liquid-storage tanks", *Finite Elem. Anal. Des.*, **37**, 467-483.
- Choi, E.Y., Cho, J.R., Cho, Y.U., Jeong, W.B., Lee, S.B., Hong, S.P. and Chun, H.H. (2015), "Numerical and experimental study on dynamic response of moored spar-type scale platform for floating offshore wind turbine", *Struct. Eng. Mech.*, **54**(5), 909-922.
- Currie, I.G. (1974), *Fundamental Mechanics of Fluids*, McGraw-Hill, New York.
- Dalzell, J.F. (1999), "A note on finite depth second-order wave-wave interactions", *Appl. Ocean Res.*, **21**, 105-111.
- Dean, R.G. and Dalrymple, R.A. (1984), *Water Wave Mechanics for Engineers and Scientists*, Prentice-Hall, Englewood Cliffs, New Jersey.
- Haslum, H.A. and Faltinsen, O.M. (1999) "Alternative shape of spar platforms for use in hostile areas", Offshore Technology, Houston, Texas, OTC-10953-MS.
- Hong, Y.P., Lee, D.Y. and Choi, Y.H. (2005), "An experimental study on the extreme motion responses of a SPAR platform in the heave resonant waves", *Proceedings of the 5<sup>th</sup> International Offshore Polar Engineering Conference*, Seoul, Korea, June.
- Irani, M.M. and Finn, L. (2004), "Model testing for vortex induced motions of spar platforms", *ASME 2004 23<sup>rd</sup> International Conference Offshore Mechanics and Arctic Engineering*, OMAE2004-51315, 605-610.
- Jeon, S.H., Cho, Y.U., Seo, M.W., Cho, J.R. and Jeong, W.B. (2013), "Dynamic response of floating substructure of spar-type offshore wind turbine with catenary mooring cables", *Ocean Eng.*, **72**, 356-364.
- Karimirad, M., Meissonnier, Q. and Gao, Z. (2011), "Hydroelastic code-to-code comparison for a tension leg spar-type floating wind turbine", *Marine Struct.*, **24**(4), 412-435.
- Kim, J.M., Chang, S.H. and Yun, C.B. (2002), "Fluid-structure-soil interaction analysis of cylindrical liquid storage tanks subjected to horizontal earthquake loading", *Struct. Eng. Mech.*, **13**(6), 615-638.
- Kriebel, D.L. (1998), "Nonlinear wave interaction with a vertical circular cylinder: wave forces", *Ocean Eng.*, **25**(7), 597-605.
- Matos, V.L.F., Simos, A.N. and Sphaier, S.H. (2011), "Second-order resonant heave, roll and pitch motions of a deep draft semi-submersible: Theoretical and experimental results", *Ocean Eng.*, **38**(17-18), 2227-2243.
- Olinger, D.J., DeStefano, E., Murphy, E. and Naqvi, S. (2012), "Scale-model experiments on floating wind turbine platforms", *50<sup>th</sup> AIAA Aerospace Sciences Meeting Including the New Horizons Forum and Aerospace Exposition*, Nashville, Tennessee, AIAA 2012-0375.
- Pinkster, J.A. (1980), *Low Frequency Second Order Wave Exciting Forces on Floating Structures*, Thesis, TU Delft.
- Rho, J.B., Choi, H.S. and Lee, W.C. (2002), "Heave and pitch motion of a spar platform with damping plate", *Proceedings of the 12th International Offshore Polar Engineering Conference*, Kitakyshu, Japan, May.
- Rho, J.B., Choi, H.S. and Lee, W.C. (2004), "Vertical motion characteristics of truss spars in waves", *Proceedings of the International Offshore Polar Engineering Conference*, Toulon, France, May.
- Sahin, I., Crane, J.W. and Watson, K.P. (1997), "Application of a panel method to hydrodynamics of underwater vehicles", *Ocean Eng.*, **24**(6), 501-512.
- Sorensen, R.M. (1978), *Basic Coastal Engineering*, John Wiley, New York.
- Utsunomiya, T., Nishida, E. and Sato, I. (2009), "Wave response experiment on spar-type floating bodies for offshore wind turbine", *Nineteenth International Offshore Polar Engineering Conference*, Osaka, Japan.

- Wang, C.Z. and Wu, G.X. (2007), "Time domain analysis of second-order wave diffraction by an array of vertical cylinders", *J. Fluid. Struct.*, 23, 605-631.
- Wang, H.F., Fan, Y.H. and Moreno, I. (2016), "Analysis of a preliminary configuration for a floating wind turbine", *Struct. Eng. Mech.*, 59(3), 559-577.
- Zhao, J., Tang, Y. and Shen, W. (2010), "A study on the combination resonance response of a classic spar platform", *J. Vib. Control*, 16, 2083-2107.

CC

## Appendix

The harmonic heave and pitch motions of the 2-DOF floating platform shown in Fig. 2 are expressed by

$$\ddot{z}(t) + \omega_h^2 z(t) = \tilde{F}_V \cdot \cos(\omega t) \quad (\text{A1})$$

$$\ddot{\theta}(t) + \omega_p^2 \theta(t) = \tilde{M} \cdot \cos(\omega t) \quad (\text{A2})$$

with  $\tilde{F}_V = F_V/m$  and  $\tilde{M} = M/m$  being the normalized vertical force and the normalized moment. For the initial conditions:  $z(0) = \dot{z}(0) = \theta(0) = \dot{\theta}(0) = 0$ , the general solutions of  $z(t)$  and  $\theta(t)$  become

$$z(t) = A \cos(\omega t) - A \cos(\omega_h t) \quad (\text{A3})$$

$$\theta(t) = B \cos(\omega t) - B \cos(\omega_p t) \quad (\text{A4})$$

with  $A = \frac{\tilde{F}_V}{\omega_p^2 - \omega^2}$  and  $B = \frac{\tilde{M}}{\omega_p^2 - \omega^2}$ . By substituting Eqs. (A3) and (A4) into  $z(t)$  in Eq. (14), one can get

$$z_G(t) = A \cos(\omega t) - A \cos(\omega_h t) + 2 \cdot \overline{GM_\theta} \cdot \sin \left[ \frac{B \cos(\omega t) - B \cos(\omega_p t)}{2} \right]^2 \quad (\text{A5})$$

Taking the Taylor series expansion to the term  $\sin[\cdot]^2$  leads to

$$z_G(t) = A \cos(\omega t) - A \cos(\omega_h t) + 2 \cdot \overline{GM_\theta} \cdot \left[ \sum_{n=1}^{\infty} (-4)^{n-1} \frac{1}{n!} \vartheta^{2n} \right] \quad (\text{A6})$$

with  $\vartheta$  being  $\frac{B \cos(\omega t) - B \cos(\omega_p t)}{2}$ . Taking the first-order term of Taylor series expansion leads to the approximate solution given by

$$z_G(t) = A \cos(\omega t) - A \cos(\omega_h t) + 2 \cdot \overline{GM_\theta} \cdot \left[ \frac{B \cos(\omega t) - B \cos(\omega_p t)}{2} \right]^2 \quad (\text{A7})$$

After the manipulation of harmonic functions, Eq. (A7) ends up with

$$z_G(t) = A \cos(\omega t) - A \cos(\omega_h t) + \frac{B^2 \cdot \overline{GM_\theta}}{4} \cos(\omega - \omega_p) [\cos(2\omega) t - 2t - 2\cos(\omega + \omega_p) t + \cos(2\omega_p) t + 2] \quad (\text{A8})$$